Applied Surface Science 256 (2010) 2372–2379

Contents lists available at ScienceDirect

Applied Surface Science

journal homepage: www.elsevier.com/locate/apsusc

Characterization of AISI 4140 borided steels

I. Campos-Silva [a,*], M. Ortiz-Domínguez [a], N. López-Perrusquia [a], A. Meneses-Amador [a], R. Escobar-Galindo [b], J. Martínez-Trinidad [a]

[a] Instituto Politécnico Nacional, Grupo Ingeniería de Superficies, SEPI-ESIME U.P. Adolfo López Mateos, Zacatenco, México D.F., 07738, Mexico
[b] Instituto de Ciencia de Materiales de Madrid (CSIC), E-28049 Cantoblanco, Madrid, Spain

ARTICLE INFO

Article history:
Received 2 October 2009
Accepted 20 October 2009
Available online 24 October 2009

Keywords:
Boriding
Growth kinetics
Characterization
Diffusion model
Fracture toughness
Hard coatings
Residual stresses

ABSTRACT

The present study characterizes the surface of AISI 4140 steels exposed to the paste-boriding process. The formation of Fe_2B hard coatings was obtained in the temperature range 1123–1273 K with different exposure times, using a 4 mm thick layer of boron carbide paste over the material surface. First, the growth kinetics of boride layers at the surface of AISI 4140 steels was evaluated. Second, the presence and distribution of alloying elements on the Fe_2B phase was measured using the Glow Discharge Optical Emission Spectrometry (GDOES) technique. Further, thermal residual stresses produced on the borided phase were evaluated by X-ray diffraction (XRD) analysis. The fracture toughness of the iron boride layer of the AISI 4140 borided steels was estimated using a Vickers microindentation induced-fracture testing at a constant distance of 25 μm from the surface. The force criterion of fracture toughness was determined from the extent of brittle cracks, both parallel and perpendicular to the surface, originating at the tips of an indenter impression. The fracture toughness values obtained by the Palmqvist crack model are expressed in the form $K_C(\pi/2) > K_C > K_C(0)$ for the different applied loads and experimental parameters of the boriding process.

1. Introduction

Boriding is a thermochemical surface treatment, in which boron is diffused into, and combines with, the substrate forming a single or double phase metal boride layer at the surface. In industry, boriding is generally applied to ferrous alloys to enhance their surface hardness and wear resistance [1]. In addition to being a selective method, the paste-based treatment reduces manual work compared with the powder-based boriding process [2,3]. Depending on the boron potential that surrounds the material surface, the chemical composition of the substrate, temperature and treatment time, two phases can be identified in the surface layer, i.e. an outer phase, FeB, with a boron content of 16 wt.%, and an inner phase, Fe_2B, with a boron content approximately of 8 wt.% [4,5]. Previously, it was found that the interfaces of FeB/Fe_2B and Fe_2B/substrate, which are present at the surface of different ferrous and nonferrous alloys in the boriding process, have a rough or saw-toothed morphology. However, when the alloying elements increase in concentration on the substrate, the formation and morphology of the growth interface at the surface of the sample tends to be flat [6].

The present study characterizes the surface of AISI 4140 steels hardened by the paste-boriding process. The evaluation of the growth kinetics of Fe_2B layers at the material surface was done at different boride incubation times to estimate the boron diffusion coefficient at the hard coatings. The GDOES technique showed the concentration profile of alloying elements that diffused in the borided phase. The XRD technique was used to estimate the magnitude and distribution of residual stresses along the boride layer. Finally, the fracture toughness of the borided phase was evaluated under the experimental parameters of 6 and 8 h of treatment for the different temperatures of the boriding process, considering the length of brittle cracks, parallel and perpendicular to the surface that originate at the tips of an indented impression.

2. Diffusion model

The growth kinetics of borided layers has received significant attention during the last 20 years for the automation and optimization of the boriding process [7–10].

In this work, some assumptions were considered for the diffusion model:

(i) The boron concentration $C_{Fe_2B}(x(t))$ at the Fe_2B phase (Fig. 1) depended only on the position $x(t)$.
(ii) The growth kinetics was controlled by the boron diffusion in the Fe_2B layer.
(iii) The growth of the boride layer occurred as a consequence of the boron diffusion perpendicular to the specimen surface.

* Corresponding author. Tel.: +52 55 57296000x54768; fax: +52 55 57296000x54589.
E-mail address: icampos@ipn.mx (I. Campos-Silva).

0169-4332/$ – see front matter © 2009 Elsevier B.V. All rights reserved.
doi:10.1016/j.apsusc.2009.10.070

(iv) The boron concentration values along the Fe_2B/substrate interface were unknown.
(v) Differences in specific volume per solvent atom for the Fe_2B phase were accommodated fully in the diffusion direction.
(vi) The influence of the alloying elements on the growth kinetics of the layer was not taken into account.

The C^{B}_{ads} is defined as the effective boron concentration at the borided layer [9]. Since only Fe phase is present before boriding, the initial condition can be written as:

$$C_{Fe_2B}(x(t>0)=0)=0$$

The boundary conditions of the problem are considered in the form:

$$C_{Fe_2B}(x(t=t_0(T))=0)=C_{up} \quad \text{for } C^{B}_{ads} > 8.83\,\text{wt.\% B}$$

$$C_{Fe_2B}(x(t=t)=u)=C_{low} \quad \text{for } C^{B}_{ads} < 8.83\,\text{wt.\% B}$$

C_{up} is the upper limit of boron concentration at Fe_2B phase and C_{low} is the lower limit of boron concentration at Fe_2B phase.

The mass balance equation at the Fe_2B/substrate interface was set as [11,12]:

$$(C_{low}-\beta C_0)\left(\frac{dx(t)}{dt}\right)\Big|_{x(t)=u} = -D_{Fe_2B}\frac{dC_{Fe_2B}(x(t))}{dx(t)}\Big|_{x(t)=u} \quad (1)$$

C_0 is the initial boron concentration in the substrate and β is the ratio of the specific volume per solvent atom, $\beta = V^{m}_{0}/2V^{m}_{Fe_2B}$ (V^{m}_{0} is the molar volume of the substrate and $V^{m}_{Fe_2B}$ is the molar volume of the Fe_2B phase (m^3/mol)).

Using the rule for differentiating compositions of functions in Eq. (1) resulted in the following equation:

$$(C_{low}-\beta C_0)\left(\frac{dx(t)}{dt}\right)\Big|_{x(t)=u} = -D_{Fe_2B}\frac{dC_{Fe_2B}(x(t))}{dt}\left(\frac{dt}{dx(t)}\right)\Big|_{x(t)=u} \quad (2)$$

Hence, Eq. (2) is rewritten as follows:

$$(C_{low}-\beta C_0)\left(\frac{dx(t)}{dt}\right)^2(dt)\Big|_{x(t)=u} = -D_{Fe_2B}dC_{Fe_2B}(x(t))|_{x(t)=u} \quad (3)$$

The growth of Fe_2B layer was governed by the parabolic growth law $x(t)=u=k(t^{1/2}-t_0^{1/2}(T))$ where u is the layer thickness, k is the parabolic growth constant, t represents the treatment time and $t_0(T)$ is the boride incubation time as a function of treatment temperature [8,13–15].

After rearranging, it follows from Eq. (3):

$$(C_{low}-\beta C_0)\frac{k^2}{4}\int_{t_0(T)}^{t}\frac{dt}{t} = -D_{Fe_2B}\int_{C_{up}}^{C_{low}} dC_{Fe_2B}(x(t))|_{x(t)=u} \quad (4)$$

The literature indicates that the upper limit of the boron concentration (C_{up}) in the Fe_2B phase is 9 wt.% B [16–18].

Assuming that the boron concentrations remained constant during the treatment at the boride layer, the D_{Fe_2B} value was determined:

$$D_{Fe_2B} = 13k^2\ln\left(\frac{t}{t_0(T)}\right) \quad (5)$$

3. Experimental procedure

3.1. Paste-boriding process

Samples of AISI 4140 commercial steel with dimensions of 8 mm × 8 mm × 5 mm were used for the thermochemical treatment. The boriding process was carried out in a conventional furnace under a pure argon atmosphere. The temperatures of 1123, 1173, 1223 and 1273 K with 2, 4, 5, 6 and 8 h were selected. Four millimeters of boron carbide paste covered the

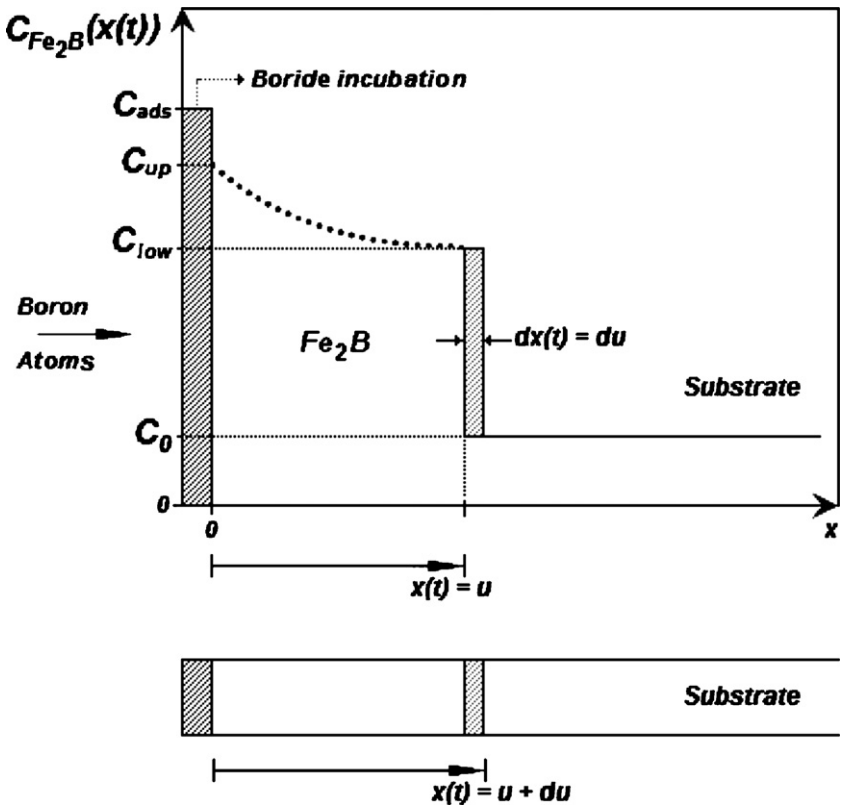

Fig. 1. Boron concentration profile for a diffusion controlled of Fe_2B into an initially homogeneous two phase alloy. The hashed area indicates amount of boron needed to advance the Fe_2B phase by *du*.

samples.[1] At the end of the boriding treatment, each sample was quenched in oil and cross-sectioned by electrical discharge machining. The metallographic preparation employed a sequence of abrasion, down to 1000-grit silicon carbide abrasion paper, followed by polishing with a diamond paste and ethylene glycol. The thicknesses of the boride layers were measured by means of optical microscopy in clear field at 250× magnification. The obtained images were analyzed using a MSQ PLUS software. The thickness measurement program was designed to measure the thickness of layers. Automatic measurements could be performed by constructing a series of parallel section lines which were combined with the thresholded image of the layer to be measured. The lengths of those portions of the section lines that overlay the selected layer were measured. For the Fe_2B layer the penetration depth was determined by selecting those needles that penetrated most deeply into the substrate. In each sample, minimum of 25 measurements were done at different points; the reported values are the average thickness of the layers.

3.2. Characterization of the boride layers by the GDOES technique

The concentration profile of the alloying elements across the Fe_2B phase was estimated by the GDOES technique using a Horiba Jobin Yvon RF GD, operating at a typical radio frequency discharge pressure of 650 Pa and 40 W power. The chamber was cleaned by sputtering a silicon sample for 20 min. Before every experiment the samples were flushed with argon for 60 s. Quantified profiles were obtained automatically using the standard Jobin Yvon QUANTUM Intelligent Quantification (IQ) software. A collection rate of 4 points/s was used to measure the samples. In order to reach depths larger than 150 μm the experimental time was set for 45 min. The analysis was carried out with the borided sample obtained at the temperature of 1223 K with 5 h of treatment.

3.3. Estimation of thermal residual stresses in boride layers

The analysis of residual stress by X-ray diffraction involves the measurement of elastic lattice strains as a function of two angles φ and ψ, where ψ is the inclination angle of the sample surface normal with respect to the diffraction vector and φ denotes the rotation of the sample around the sample surface normal (for more information see Ref. [19]). The tests were done using the XSTRESS3000 X-ray equipment with a CrK_α radiation, with a diffraction angle of $2\theta = 156.4^\circ$ (wavelength $\lambda = 2.28$ A) operating at 30 kV. AISI 4140 borided samples obtained at the temperatures of 1173, 1223 and 1273 K with 8 h of exposure time were selected for this purpose. The ψ tilt angles were set between -45° and $+45^\circ$ and the φ angles were established in 0° and 90°. In each rotation angle, eight measurements on different ψ angles were performed. To obtain a residual stress–depth profile, the surface of the borided steels was removed by electrolytic polishing, and the stresses on each 10 μm were measured. The reference values of modulus and Poisson's ratio used in the calculations were taken from [20].

3.4. Induced-fracture by Vickers microindentation

The wear resistance of borided layers is related to the fracture toughness of the borided phases. The method of microindentation induced-fracture in brittle materials is a nondestructive and simple technique, which requires only a flat and polished surface. The cracks produced by mechanical contact between the indenter and the material surface, essentially depend on the geometry of the indenter and the applied load.

[1] The boron carbide paste ($B_4C + Na_3AlF_6$) was mixed with distilled water with a 0.2 ratio (boron carbide paste/water).

The cracks geometry models, i.e. radial-median and Palmqvist types, have been used in the determination of the fracture toughness in ceramic materials. The theoretical foundation of these models was based on classic concepts of Linear Elastic Fracture Mechanics (LEFM) (see [21,22] and references therein). For the Palmqvist cracks regime (Fig. 2), it has been determined for small loads, that the relation between the half diagonal length of the indentation (d) and the crack length generated at the corners of the indentation (a) must be ≤ 3. This seemed to be a reasonable assumption for brittle layers on relatively tough substrates. However, for the case of borided steels, it would be more appropriate to use the relationships based on the Palmqvist crack morphology, as this model was based on cracking initiating at the surface where the material was more brittle. In the work presented by Shetty et al. [23], they proposed an empirical model in the Palmqvist crack regime for the evaluation of the fracture toughness (K_C) on ceramic materials:

$$K_C = 0.0319\left(\frac{P}{d\sqrt{a}}\right) \tag{6}$$

where P is the indentation load.

The Vickers microindentation fracture toughness tests were performed with a HVS 1000 microhardness tester, using the ASTM E384 standard. Borided samples obtained at the temperatures of 1123, 1173, 1223 and 1273 K with 6 and 8 h were selected for this purpose. Note that the samples were selected in accordance with

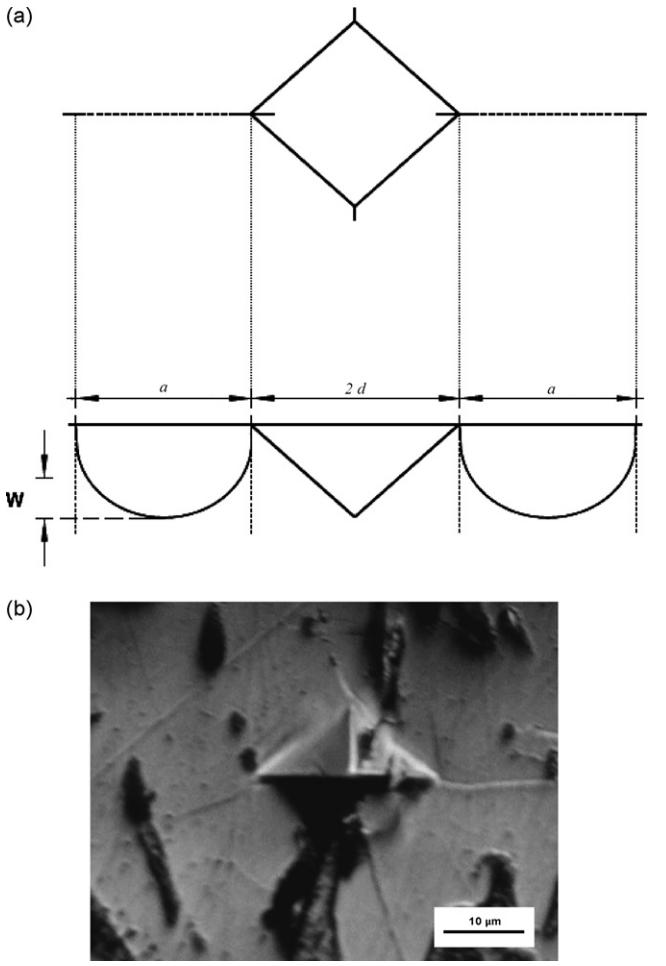

Fig. 2. (a) Palmqvist cracks around the Vickers indentation and (b) fracture indentation testing over the Fe_2B layer created at the surface of AISI 4140 borided steel.

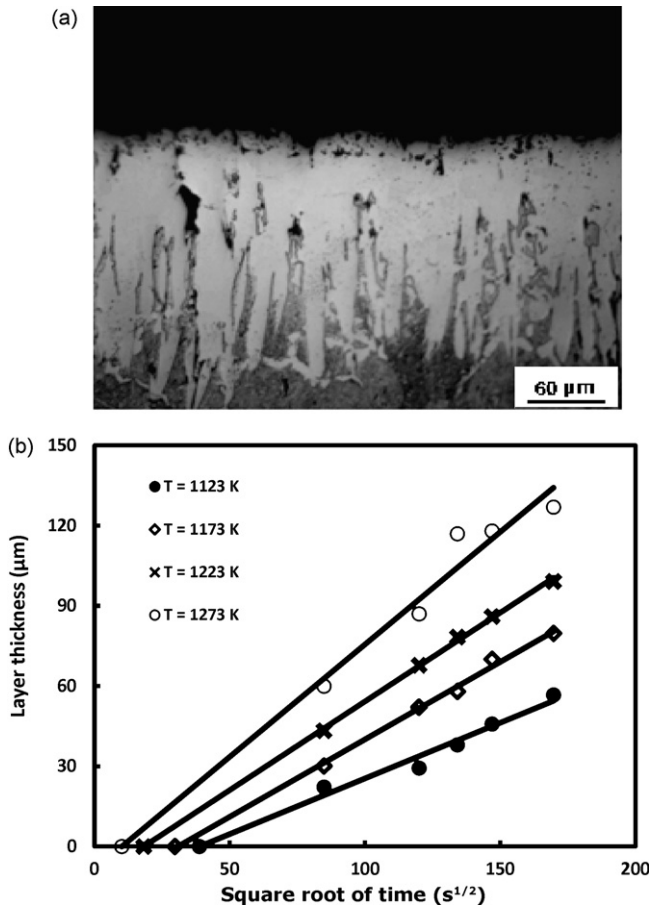

Fig. 3. (a) Cross-sectional view of the surface of AISI 4140 steel boriding at the temperature of 1273 K with 8 h of treatment and (b) evolution of the boride layer thickness as a function of square root of time.

the Fe_2B layer thicknesses. The indentation loads were varied between 1.9 and 9.8 N applied at 25 μm from the surface. Ten measurements were taken for each load, time and temperature of the process.

For the estimation of the fracture toughness of the borided phase, both Vickers diagonals (d) and crack lengths[2] (a) were measured in an Olympus GX 51 optical microscope. The Young modulus used for the borided layers was 290 GPa [20].

4. Results and discussions

4.1. Growth kinetics of boride layers

The Fe_2B layers formed at the surface of the AISI 4140 steels exhibited needle-like growth similar to those found in borides created in low-alloy steels (Fig. 3(a)), due to the anisotropic nature of the diffusion in the Fe_2B phase. Also, the Fe_2B layer was shown to exhibit a (0 0 1) texture that became increasingly sharp for increasing penetration depths (see [8] and references therein). As the metal surface was covered, an increasing number of Fe_2B crystals came into contact with adjacent crystals and were forced to grow inside the metal, retaining an acicular shape. Hence, the growth of the boride grains with other orientations was slower and soon suppressed as they met other grains, resulting in an overall ⟨0 0 1⟩ texture structure.

[2] The fracture toughness values were obtained by the measurement of the crack lengths at the corners of the indentation prints in parallel and perpendicular directions to the surface.

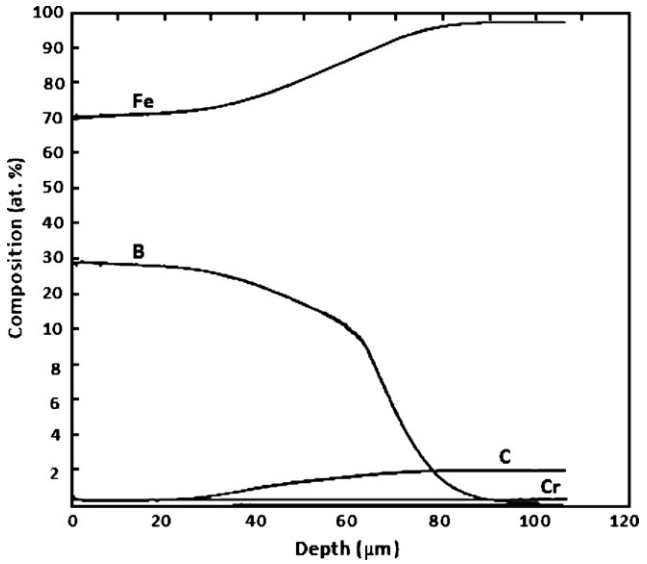

Fig. 4. Quantitative GDOES profile obtained at the surface of AISI 4140 borided steel at the temperature of 1223 K with 5 h.

Assuming that the growth of the Fe_2B layer was controlled by the boron diffusion perpendicular to the surface (for the boride layers [0 0 1] appeared to be the easiest diffusion direction) and obeyed the parabolic growth law, the growth constants k were evaluated from the straight lines obtained in Fig. 3(b), considering the boride incubation time $t_0(T)$ at the surface of the AISI 4140 steel. It is visible from Fig. 3(b), the higher the temperature, shorter the boride incubation time.

The GDOES profile corresponding to the borided sample with 5 h and 1223 K (Fig. 4) showed that the carbon was displaced to the diffusion zone, and tended to form boron cementite with the substrate, according to Goeuriot et al. [24]. On the other hand, at the distance of 15 μm, the chromium dissolved into the boride layer was observed. It was established by Carbucicchio and Palombarini [25] that Cr was concentrated in the boride layer to form CrB, which has a crystalline structure similar to the Fe_2B phase. Likewise, the value of boron surface concentration gradually decreased from 30 at.% until it reached a minimum at the layer/substrate interface. This observation indicated that the matrix beneath the boride layer was enriched by boron atoms. It should be noted that the boron concentration profile of the borided samples did not exactly match at different locations due to the roughness of the boride layer/substrate interface, which arises from the saw-toothed morphology of the boride layer.

The boron diffusion coefficient at the Fe_2B phase was determined by Eq. (5), using the corresponding growth constant values, the boride incubation and treatment times. Assuming that the boron diffusion coefficient (D_{Fe_2B}) is dependent on the treatment temperature, the activation energy Q could be derived from the slope of the straight line obtained by plotting $\ln D_{Fe_2B}$ as a function of the reciprocal boriding temperature as shown in Fig. 5. The boron diffusion coefficient is expressed as:

$$D_{Fe_2B} = 5.4 \times 10^{-4} \exp\left(-\frac{173 \times 10^3\,\mathrm{J\,mol^{-1}}}{RT}\right)(\mathrm{m^2\,s^{-1}}) \quad (7)$$

The Q value indicates the amount of energy for the boron mobility in the easiest path direction [0 0 1] along the borided phase. The activation energy value was compared with the experimental data (Table 1) obtained in other works. Table 1 shows that the amount of energy required for stimulating the formation of the boride layer increased for high alloy steels.

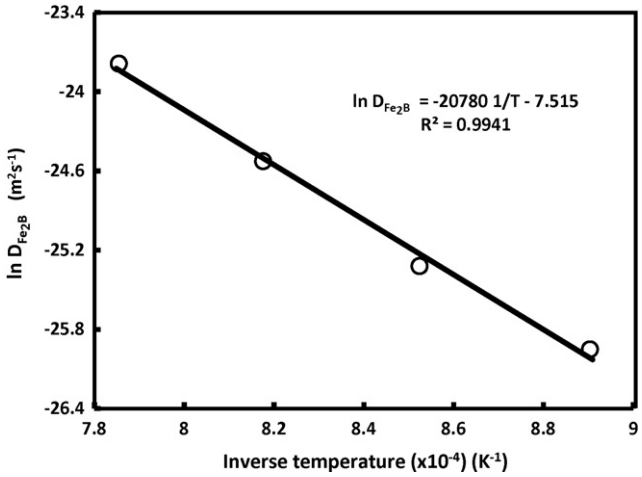

Fig. 5. Dependence between the boron diffusion coefficient (D_{Fe_2B}) and the treatment temperature.

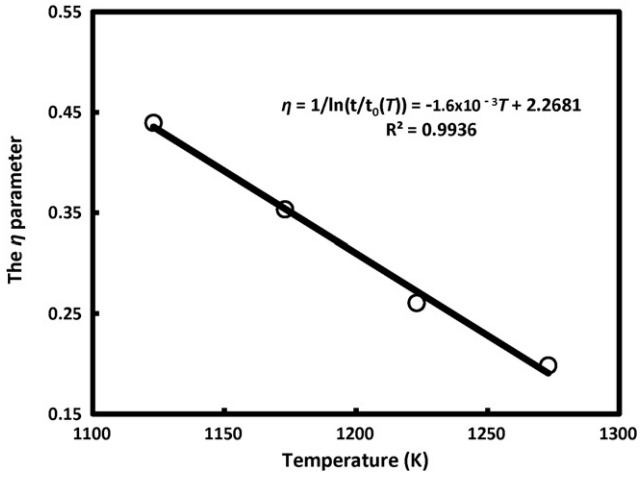

Fig. 6. Influence of the temperature on the η parameter.

Table 1
Comparison between activation energy values on different borided steels.

Borided sample	Q (kJ mol^{-1})	Reference
ARMCO iron	156	[8]
AISI 5140 steel	223	[10]
AISI 1040	168	[34]
AISI 4140	173	Present work

For the paste-boriding process, the growth kinetics of the boride layers is a function of the variability of the boron paste thickness over the material surface. The increased paste thickness is reflected in the higher boron mobility in boride phases (under constant treatment temperature) and in a reduction of the activation energy [26,27].

The evolution of k as a function of boron concentration in the Fe_2B phase and of boride incubation time is established from Eq. (5):

$$k^2 = \frac{4}{\ln(t/t_0(T))}\left(\frac{C_{up}-C_{low}}{C_{low}-\beta C_0}\right)D_{Fe_2B} \quad (8)$$

$$k^2 = \frac{\eta D_{Fe_2B}}{13}\ (m^2\,s^{-1}) \quad (9)$$

where

$$\eta = \frac{1}{\ln(t/t_0(T))} = -1.6\times10^{-3}T + 2.2681 \quad (10)$$

The parameter $1/\ln(t/t_0(T))$ has no physical dimension, depends only on the boriding temperature and can be approximated by a linear relationship as shown in Fig. 6.

From Eq. (9) and the results shown in Figs. 5 and 6, the parabolic growth constant may then be expressed as:

$$k^2 = (-1.6\times10^{-3}T + 2.2681)\frac{5.4\times10^{-4}\exp(-173\times10^3\,J\,mol^{-1}/RT)}{13} \quad (11)$$

and results in:

$$k = 3(1\times10^{-3}T - 1)\,(m\,s^{-1/2}) \quad (12)$$

Fig. 7 illustrates the evolution of the parabolic growth constant as a function of boriding temperatures. The data are summarized in Table 2, and are in good agreement with the experimental growth constants obtained in this work.

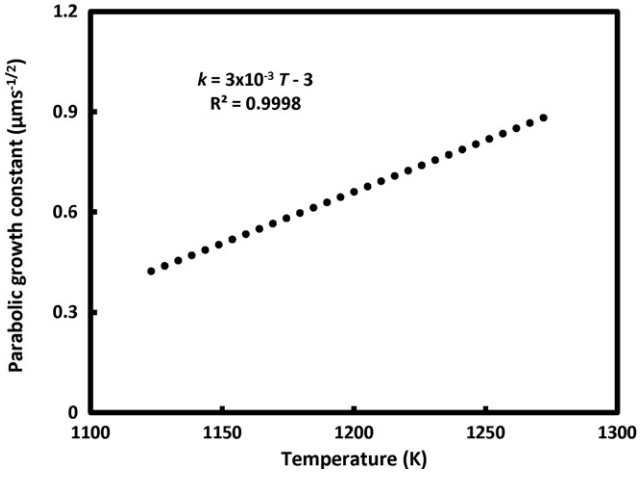

Fig. 7. Parabolic growth constant as a function of boriding temperature.

4.2. Residual stresses in AISI 4140 borided steels

The measurements of residual stresses obtained at the Fe_2B layers were conducted as a function of boriding temperatures and rotation angle φ as shown in Fig. 8. One of the most important parameters to consider in the formation of residual stresses at the boride layer was the difference in thermal expansion values between the layer and the substrate. On cooling, the substrate shrinks more than the boride layer due to its larger coefficient of linear expansion. As a consequence, a thermally induced compressive strain had to be imposed to the layer to attach the layer onto the substrate at the temperature below the boriding temperature [28]. Also, as stated by Babushkin and Polyakov [29], the magnitude and distribution of residual stresses depend, to a considerable extent, on

Table 2
Experimental and predicted values of the parabolic growth constants in the temperature range 1123–1273 K.

Temperature (K)	Experimental growth constants ($\mu m\,s^{-1/2}$)	Predicted growth constants ($\mu m\,s^{-1/2}$)
1123	0.416	0.369
1173	0.515	0.519
1223	0.663	0.669
1273	0.840	0.819

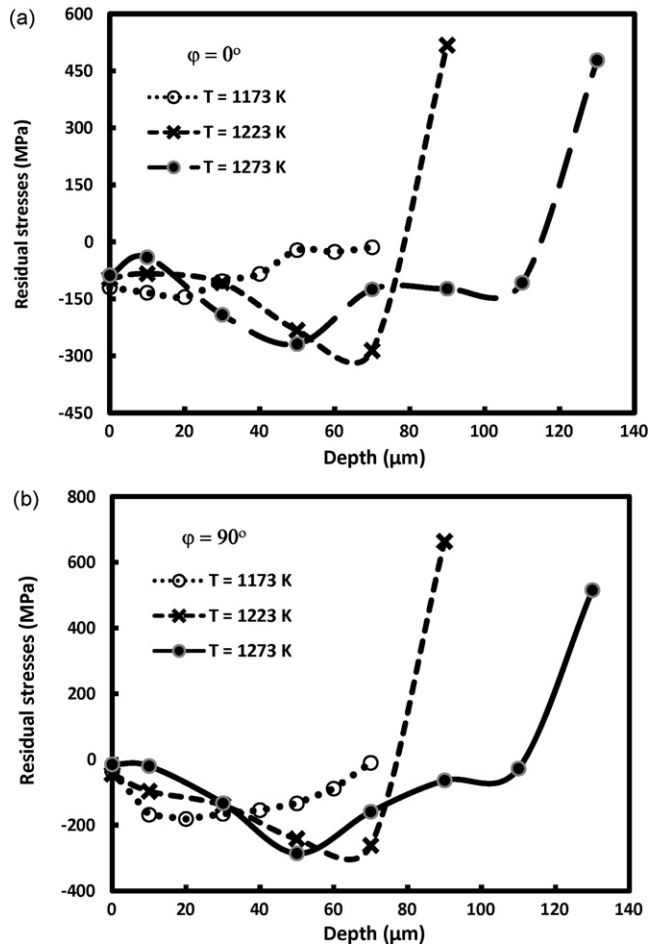

Fig. 8. Residual stress distribution across boride coatings on AISI 4140 steels measured for rotation angles (φ) of (a) 0° and (b) 90°.

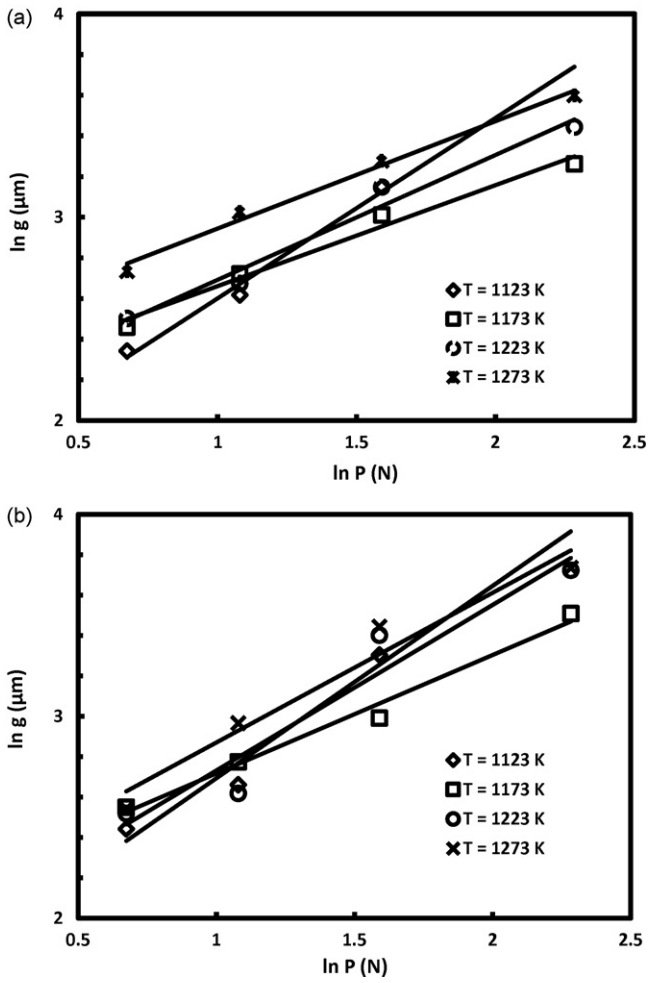

Fig. 9. Relationship between the crack length and the Vickers indentation loads obtained in AISI 4140 borided steels at treatment times of (a) 6 h and (b) 8 h.

the phase composition of the boride coating, the technique of the layer production, and the process parameters. The experiments performed have shown (Fig. 8) that the stresses occurring in the continuous Fe_2B layer were compressive and highly anisotropic and decreased as a function of the penetration depth. Furthermore, the stresses switched from compressive to tensile toward the boride to steel substrate interface. The magnitude of compressive stresses for both rotation angles observed in the near-surface region of the borided steels peaked when the temperature increased. In this case, compressive stresses observed at Fe_2B layers, improved performance of different mechanical components and also the capacity for static tensile loads while, tensile stresses could have a detrimental effect [30].

4.3. Microindentation fracture toughness results

The presence of Palmqvist cracks that originated at the corners of the Vickers indentation in borided steels, and obtained for a set of experimental parameters, was confirmed from the graph of ln P versus ln g (Fig. 9), in which, the slopes were between 1/2 and 1. The values indicate semi-infinite cracks loaded by a force P at a distance g from the crack tip (see [31] and references therein). The microhardness mean values obtained at 25 μm from the surface of the Fe_2B layer (considering the boriding temperatures) were estimated to be 1604 ± 207 HV (for 6 h exposure time), and 1672 ± 176 HV (for 8 h of exposure time). The hardness values were used to evaluate the mechanical support of the Fe_2B phase.

The behavior of K_C as a function of the indentation load is shown in Fig. 10 and summarized in Table 3. Due to the anisotropy and non-uniformity of the boride layer, the fracture toughness values were obtained in the form of the function $K_C(\theta)$, where θ is the coordinate angle between the direction of crack propagation and the surface. In this case, the experimental values of the function $K_C(\theta)$ in the Fe_2B layers corresponded to the directions in which the angle θ was 0 and $\pi/2$. At first instance, the graphs show that the fracture toughness of Fe_2B phase was independent of the applied load in the two directions corresponding to the crack propagation at the corners tips. Furthermore, the results suggest that the fracture toughness decreased with increasing treatment time, and that the K_C values corresponding to the direction of $\pi/2$ were higher than the values obtained in the parallel direction. Investigations have shown [32,33] that in coatings consisting of columnar grains elongated in the direction of the surface, the anisotropy of the brittle strength was characterized by the relationship of the extreme values of fracture toughness $K_C(\pi/2) > K_C(0)$. This behavior was a consequence of high compressive residual stresses normal to the surface region (see Fig. 8) that decreased the crack length in the preferential [0 0 1] growth direction. The degree of anisotropy of the fracture resistance obtained in boride layers can be evaluated as:

$$\frac{K_C(\pi/2) - K_C(0)}{K_C(0)} \tag{13}$$

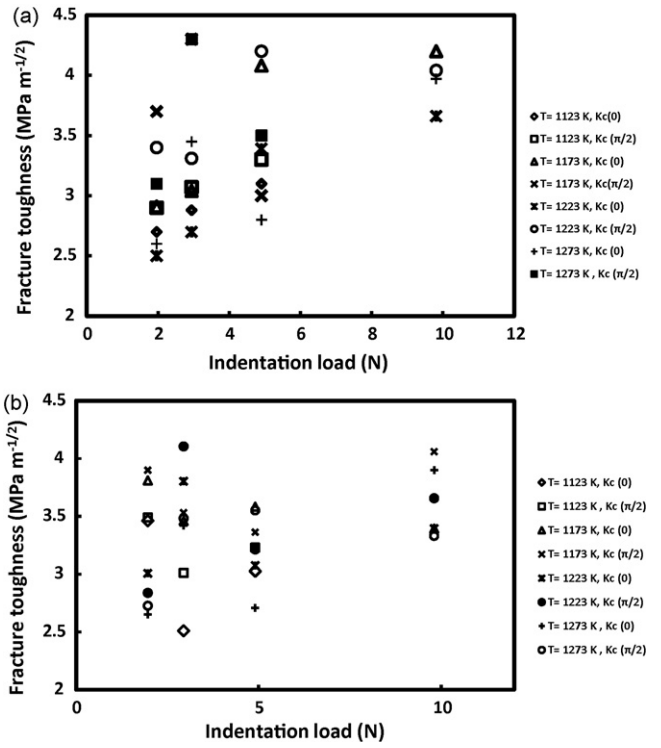

Fig. 10. Behavior of fracture toughness values of Fe_2B layer against the indentation load for exposure times of (a) 6 h and (b) 8 h.

Table 3
Anisotropy of fracture resistance obtained on Fe_2B layers.

Temperature (K)	Time (h)	$K_C(0)$ ($MPa\,m^{1/2}$)	$K_C(\pi/2)$ ($MPa\,m^{1/2}$)	Anisotropy degree (%)
1123	6	2.9 ± 0.2	3.0 ± 0.2	6.8
	8	3.0 ± 0.5	3.2 ± 0.2	8.1
1173	6	3.5 ± 0.6	4.0 ± 0.6	11
	8	3.5 ± 0.1	3.7 ± 0.3	4.2
1223	6	3.0 ± 0.5	3.7 ± 0.5	22
	8	3.3 ± 0.3	3.4 ± 0.5	4
1273	6	3.2 ± 0.4	4.0 ± 0.4	23.2
	8	3.1 ± 0.6	3.2 ± 0.4	3.2

The formation of compact layers with a higher axial texture [0 0 1] for 8 h of treatment probably decreased the degree of anisotropy of the fracture resistance on both crack directions (normal and parallel to the surface) obtained in Fe_2B layers as shown in Table 3.

5. Conclusions

The present study characterized the surface of AISI 4140 borided steels. The boron diffusion coefficient at Fe_2B coating was estimated by the mass balance equation at the growth interface and the measurement of the boride layer thicknesses as a function of temperature and boriding time. Furthermore, the growth constant k was proposed as a function of the parameter η that considers the influence of the temperature over the boride incubation time. The growth constants predicted by the model showed good agreement with the experimental data obtained for the boriding temperatures. The model is an alternative to stimulate the automation of the boriding process with different experimental data.

The residual stresses acting on the surface of the Fe_2B layer were compressive with highest stress at the near-surface region. For both rotation angles (0 and $\pi/2$ rad) the magnitude of the residual stresses at the surface increased as a function of the temperature.

The fracture resistance obtained in both crack directions was a result of non-uniform composition, morphological anisotropy of the borided phase, and the residual stresses along the surface. The results show that the fracture toughness of the Fe_2B layer can be represented by $K_C(\pi/2) > K_C > K_C(0)$ for a complete evaluation of the brittle strength of the hard coatings.

Acknowledgements

This work has been supported by the research grants 53859 of Consejo Nacional de Ciencia y Tecnología and PIFUTP08-84 of *Instituto de Ciencia y Tecnología del Distrito Federal* at Mexico. I. Campos thanks the project 20090010 chair supported by the *Secretaría de Investigación y Posgrado* of the Instituto Politécnico Nacional.

References

[1] A.K. Sinha, Boronizing, in: ASM Handbook, J. Heat Treat., USA, 1991.
[2] G. von Matuschka, Boronizing, First ed., Carl Hanser Verlag, Germany, 1980.
[3] E. Meléndez, I. Campos, E. Rocha, M.A. Barrón, Structural and strength characterization of steels subjected to boriding thermochemical process, Mater. Sci. Eng. A 234–236 (1997) (1997) 900–903.
[4] S.C. Singhal, A hard diffusion boride coating for ferrous materials, Thin Solid Films 45 (1997) 321–329.
[5] G. Wahl, Durferrit-Technical Information VDI-Z117, 1975, p. 785.
[6] I. Campos, J. Oseguera, U. Figueroa, J.A. García, O. Bautista, G. Kelemenis, Kinetic study of boron diffusion in the paste boriding process, Mater. Sci. Eng. A 352 (2003) 261–265.
[7] I. Campos, G. Ramírez, U. Figueroa, C. VillaVelázquez, Paste boriding process: evaluation of boron mobility on borided steels, Surf. Eng. 23 (2007) 216–222.
[8] C.M. Brakman, A.W.J. Gommers, E.J. Mittemeijer, Boriding of Fe and Fe–C, Fe–Cr, and Fe–Ni alloys: boride layer growth kinetics, J. Mater. Res. 4 (1989) 1354–1370.
[9] L.G. Yu, X.J. Chen, K.A. Khor, G. Sundararajan, FeB/Fe_2B phase transformation during SPS pack-boriding: boride layer growth kinetics, Acta Mater. 53 (2005) 2361–2368.
[10] S. Sen, U. Sen, C. Bindal, An approach of kinetic study of borided steels, Surf. Coat. Technol. 191 (2005) 274–285.
[11] I. Campos-Silva, M. Ortíz-Domínguez, C. VillaVelázquez, R. Escobar, N. López, Growth kinetics of boride layers: a modified approach, Defect Diffus. Forum 272 (2007) 79–86.
[12] P. Shewmon, Diffusion in Solids, Second ed., Minerals, Metals and Materials Society, USA, 1998.
[13] O. Torun, Boriding of nickel aluminide, Surf. Coat. Technol. 202 (2008) 3549–3554.
[14] C. Martini, G. Palombarini, M. Carbucicchio, Mechanism of thermochemical growth of iron borides on iron, J. Mater. Sci. 39 (2004) 933–937.
[15] I. Campos-Silva, M. Ortiz-Domínguez, M. Keddam, N. López-Perrusquia, A. Carmona-Vargas, M. Elias-Espinosa, Kinetics of the formation of Fe_2B layers in gray cast iron: effects of boron concentration and boride incubation time, Appl. Surf. Sci. 255 (2009) 9290–9295.
[16] B. Hallemans, P. Wollants, J.R. Ross, Thermodynamic reassessment and calculation of the Fe–B phase diagram, Z. Metallkd. 85 (1994) 676–682.
[17] T. Van Rompaey, K.C. Hari Kumar, P. Wollants, Thermodynamic optimization of the B–Fe system, J. Alloys Compd. 334 (2002) 173–181.
[18] M. Keddam, A kinetic model for the borided layers by the paste-boriding process, Appl. Surf. Sci. 236 (2004) 451–455.
[19] U. Welzel, J. Ligot, P. Lamparter, P. Vermeulen, E. Mittemeijer, Stress analysis of polycrystalline thin films and surface regions by X-ray diffraction, J. Appl. Cryst. 38 (2005) 1–29.
[20] N. Frantzevich, F.F. Voronov, S.A. Bakuta, Elastic Constants and Elastic Modulus for Metals and Non-metals: Handbook, First ed., Naukova Dumka Press, Kiev, 1982 .
[21] C.B. Ponton, R.D. Rawlings, Vickers indentation fracture test. Part 1: review of literature and formulation of standardised indentation toughness equations, Mater. Sci. Technol. 5 (1989) 865–872.
[22] C.B. Ponton, R.D. Rawlings, Indentation fracture toughness test. Part 2: application and critical evaluation of standardised indentation toughness equations, Mater. Sci. Technol. 5 (1989) 961–976.
[23] D.K. Shetty, I.G. Wright, P.N. Mincer, A.H. Clauer, Indentation fracture of WC-Co cermets, J. Mater. Sci. 20 (1985) 1873–1882.
[24] P. Goeuriot, R. Fillit, F. Thevenot, J.H. Drive, H. Bruyas, The influence of alloying element additions on the boriding of steels, Mater. Sci. Eng. 55 (1982) 9–19.

[25] M. Carbucicchio, G. Palombarini, Effect of alloying elements on the growth of boride coating, J. Mater. Sci. Lett. 6 (1987) 1147–1149.
[26] I. Campos, O. Bautista, G. Ramírez, M. Islas, J. de la Parra, L. Zuñiga, Effect of boron paste thickness on the growth kinetics of Fe_2B layers during the boriding process, Appl. Surf. Sci. 243 (2006) 429–436.
[27] I. Campos, G. Ramírez, U. Figueroa, J. Martínez, O. Morales, Evaluation of boron mobility on the phases FeB, Fe_2B and diffusion zone in AISI 1045 and M2 steels, Appl. Surf. Sci. 253 (2007) 3469–3475.
[28] M.A.J. Somers, Modelling nitriding of iron: from thermodynamics to residual stress, J. Phys. IV France 120 (2004) 21–33.
[29] B.V. Babushkin, P.Z. Polyakov, Residual stresses in steel after boriding from melts, Metallovedenie i Termicheskaya Obrabotka Metallov 7 (1973) 27–30.
[30] R. Prummer, W. Pfeiffer, Residual stresses in borided layers, J. Less Common Met. 117 (1986) 411–414.
[31] I. Campos, R. Rosas, U. Figueroa, C. VillaVelázquez, A. Meneses, A. Guevara, Fracture toughness evaluation using Palmqvist crack models on AISI 1045 borided steels, Mater. Sci. Eng. A 488 (2008) 562–568.
[32] A.V. Byakova, Influence of texture on the strength and supporting capacity of boride coatings, Poroshkovaya Metallurgiya 4 (1993) 36–43.
[33] A.V. Byakova, V.G. Gorbach, Fracture toughness and evaluation of coating strength with an initial residual stress field, Probl. Prochn. 1 (1994) 51–61.
[34] I. Uslu, H. Comert, M. Ipek, F.G. Celebi, O. Ozdemir, C. Bindal, A comparison of borides formed on AISI 1040 and AISI P20 steels, Mater. Des. 28 (2007) 1819–1826.